Supporting Information

Unveiling the origin of photo-induced enhancement of oxidation catalysis at Mo(VI) centres of Ru(II)-Mo(VI) dyads

Maryam Nazari Haghighi Pashaki[a], Tae-Kyu Choi[b], Egmont Rohwer[a], Thomas Feurer[a], Anne-Kathrin Duhme-Klair[c*], Wojciech Gawelda[def*], Andrea Cannizzo[a*]

[a] Institute of Applied Physics, University of Bern, Sidlerstrasse 5, CH-3012, Bern, Switzerland

[b] European XFEL, Holzkoppel 4, 22869 Schenefeld, Germany

[c] Department of Chemistry, University of York, Heslington, York YO10 5DD, UK

[d] Departamento de Química, Facultad de Ciencias, Universidad Autónoma de Madrid, Campus Cantoblanco, 28049 Madrid, Spain

[e] Instituto Madrileño de Estudios Avanzados en Nanociencia (IMDEA-Nanociencia)

Campus Cantoblanco, 28049 Madrid, Spain

[f] Faculty of Physics, Adam Mickiewicz University, ul. Uniwersytetu Poznańskiego 2, 61-614 Poznan, Poland

AUTHOR INFORMATION

Corresponding Authors

*andrea.cannizzo@iap.unibe.ch

*Anne.Duhme-Klair@york.ac.uk

*wojciech.gawelda@uam.es

Author contribution: Maryam Nazari Haghighi Pashaki, Tae-Kyu Choi, Egmont J. Rohwer and Andrea Cannizzo performed the TA experiment and the data analysis. Anne-Kathrin Duhme-Klair provided and characterized the sample by means of steady-state measurements. The scientific interpretation of the data, the final model and the manuscript were done through contributions of all authors.

Table of Contents

1. Materials and Methods

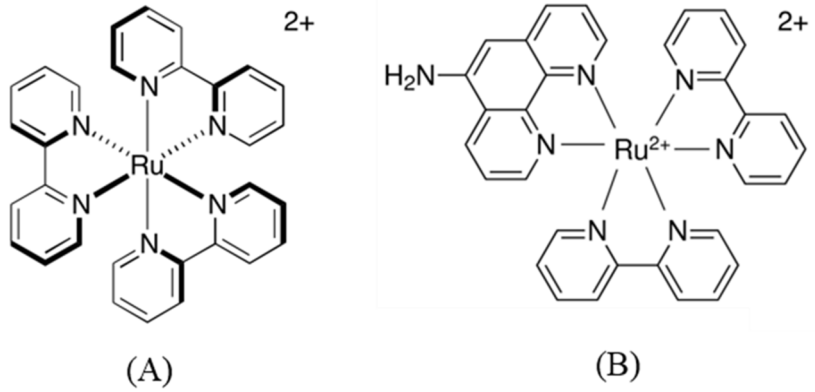

Scheme 1: Molecular structures of: (A) $[Ru(bpy)_3]^{2+}$, (B) $[Ru(bpy)_2(phen-NH_2)]^{2+}$. The respective counterions are $2Cl^-$ and $2PF_6^-$

Sample preparation. The Ru(II)-Mo(VI) dyad and $[Ru(bpy)_2(phen-NH_2)]^{2+}$ were synthesized according to[1] and dissolved in MeCN. To avoid the bleaching effect of oxygen the dyad solution was degassed for 10 mins, using Argon gas. The maximum of the ruthenium-based MLCT (Metal-to-Ligand Charge Transfer) band is at ~450 nm (Figure S1). However, due to tunability limitation of the excitation source, excitation at this wavelength was not feasible and rather samples were excited at 425 nm. To reach an optical density of ~0.1 to 0.3 OD at ~425 nm in a 200 μm optical path, solutions were prepared with a concentration of ~0.5 mM and 1.2 mM for the dyad (ε_{455} = 21700 M^{-1} cm^{-1}) and $[Ru(bpy)_2(phen-NH_2)]^{2+}$ (ε_{449} = 15700 M^{-1} cm^{-1}), respectively. To avoid photoaccumulation of sample and multiple excitations during transient absorption measurements, solutions were flowed by a micro-gear pump (mzr-2505).

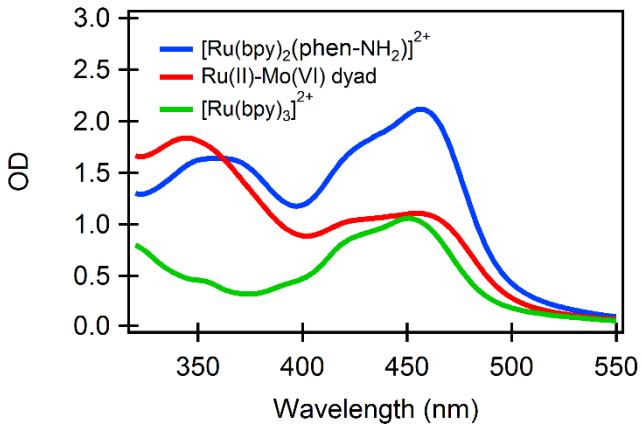

Figure S1: Steady state UV-Vis absorption spectra of the Ru(II)-Mo(VI) dyad $[Ru(bpy)_2(L)MoO_2(MeOH)]^{2+}$, $[Ru(bpy)_2(phen\text{-}NH_2)]^{2+}$ and $[Ru(bpy)_3]^{2+}$. Bands at $\lambda < 350$ nm and ~ 455 nm are MLCT transitions, mainly representing a Ru→phen MLCT and a Ru→bpy MLCT transition, respectively.

Femtosecond transient absorption spectroscopy. To generate pump pulses at 425 nm, first a fundamental 850 nm pulse was generated by a commercial non-collinear optical parametric amplifier (Topas White by Light conversion), pumped by 800 nm pulses with 0.5 mJ energy and 100 fs pulse duration from a 5 KHz Ti:Sapphire chirped pulse amplifier (Legend Elite by Coherent). Then, by focusing the collimated 850 nm into a BBO crystal (250 µm thickness) and by means of second harmonic generation at the right phase-matching angle, we generated pulses at ~ 425 nm ($\Delta\lambda$ ~ 3 nm) for excitation. Afterwards, the 850 nm residual was filtered out by a BG38 filter and the pump pulse was focused to a ca. 50 µm diameter spot size ($1/e^2$). The dyad and $[Ru(bpy)_2(phen\text{-}NH_2)]^{2+}$ were excited by pulses with 40 nJ and 100 nJ energy per pulse, respectively. A power dependence measurement was regularly carried out to ensure that experiments are conducted in a linear absorption regime.

The probe pulse was a broadband continuum covering from 320 nm to 720 nm, generated by focusing a fraction of the Ti:Sapphire laser source into a 5 mm thick CaF_2 crystal. The time resolution of the measurement was ~30 fs. More details on the set up and calculation of TA signal in a single-shot detection scheme can be found in the literature.[2]

Data analysis of time-resolved spectra. To analyse the data we adopted Singular Value Decomposition and Global Fit (SVD-GF) analysis[3] of the transient absorption data, $TA(\lambda, t)$, to separate noise, $\Xi(\lambda, t)$, from the spectral evolution of the system, $\widehat{TA}(\lambda, t)$:

$$TA(\lambda, t) = \widehat{TA}(\lambda, t) + \Xi(\lambda, t) \qquad \text{eq. 1}$$

We decomposed the latter as an expansion of exponential decays with characteristic lifetimes (τ_k) and decay associated spectra (DASs):

$$\widehat{\mathrm{TA}}(\lambda, t) = \sum_{k=1}^{k=p} \mathrm{DAS}_k(\lambda)\, e_{t>0}^{-\frac{t}{\tau_k}} |_{\mathrm{IRF}(K,t_0,t)} \qquad \text{eq. 2}$$

$e_{t>0}^{-t/\tau_k} |_{\mathrm{IRF}(K,t_0,t)}$ represents an exponential decay with decay constant τ_k multiplied by a Heaviside unit step function $u_0(t)$ and then convoluted with an instrument response function (IRF), supposed Gaussian (at time zero, t_0, and with a full width at half maximum of K).

2. Transient Absorption Measurements on $[Ru(bpy)_2(phen\text{-}NH_2)]^{2+}$ and Comparison with $[Ru(bpy)_3]^{2+}$ and the Ru(II)-Mo(VI) Dyad

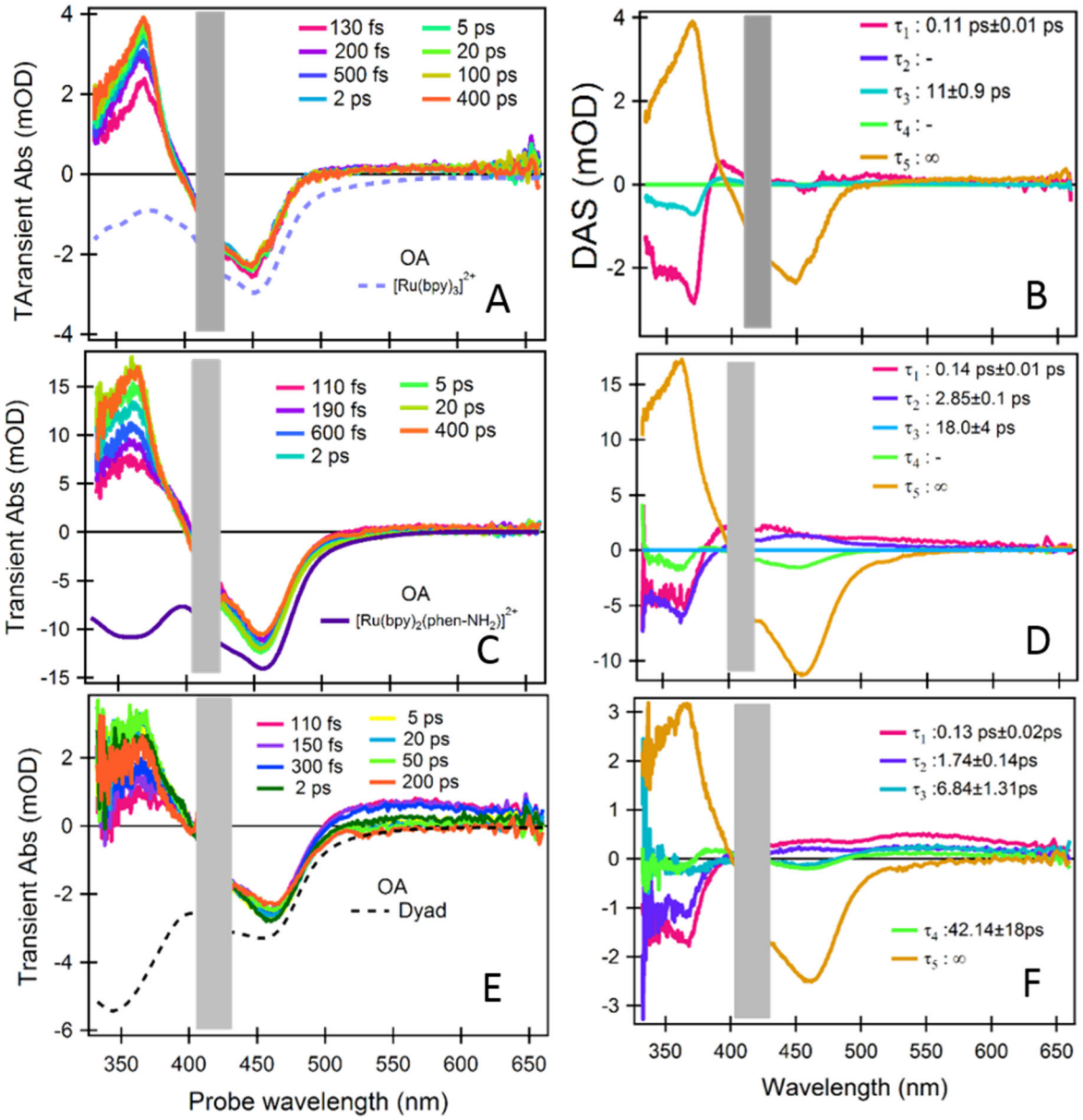

Figure S2: A representative selection of spectra obtained upon excitation at 425 nm of $[Ru(bpy)_3]^{2+}$, $[Ru(bpy)_2(phen\text{-}NH_2)]^{2+}$ and the Ru(II)-Mo(VI) dyad (left panels A, C, E, respectively). Inverted and normalized steady state absorption spectra (OA) of $[Ru(bpy)_3]^{2+}$, $[Ru(bpy)_2(phen\text{-}NH_2)]^{2+}$ and the Ru(II)-Mo(VI) dyad are shown together (from Figure S1). Respective time-spectrum decomposition analysis (right panels B, D, F, see eq. S2): decay associated spectra (DASs) and the relevant decay time constants are shown. To facilitate the inter-comparison of the analysis, the number of spectral components (τ_n) was kept constant and the ones that were not used during the analysis are labelled with "-". The spectral range contaminated by pump scattering is masked by a grey box.

We performed a comparative study of the Ru(II)-Mo(VI) dyad $[Ru(bpy)_2(L)MoO_2(MeOH)]^{2+}$, its reference $[Ru(bpy)_2(phen\text{-}NH_2)]^{2+}$ and $[Ru(bpy)_3]^{2+}$ upon excitation at 425 nm (namely Ru-bpy and Ru-phen MLCT transitions) with fs transient absorption (TA) spectroscopy (for details of measurements and sample treatment see section S1). The comparison allowed us to separate the dynamics of Ru(III)-bpy^-/$phen^-$ MLCT states from signals due to the Mo-based unit. Figure S2 reports a representative selection of TA spectra for the three complexes.

To show the consistency of the time-spectrum decomposition analysis, reconstructed kinetics at relevant wavelengths are compared with the respective experimental data in Figure S3. The chosen wavelengths are 370 nm, 460 nm and 550 nm. The first two report on the dynamics of the metal-to-ligand charge transfer states and of the ground state bleach of the Ru moiety, respectively. 550 nm tracks down the oxidative process at the Mo unit. It is worth noticing that the quality of the fitting of the dyad at the wavelength representative of the oxidative process in panel C, is very good but not excellent. As commented in the main text this is a manifestation of the fact that the oxidation dynamics are multi-exponential and spanning from 2 to 60 ps. Adding more exponential components improves the graphical quality but not the statistical quality (we observe a generalized increase the uncertainties of all the other parameters) of the fitting and it would not change the data interpretation.

In Figure S2A we observe the characteristic signatures of a Ru-to-bpy MLCT transition[4]: i) a negative signal at 450 nm indicating the ground state bleach (GSB) of excited Ru-bpy MLCT transition; ii) a positive, excited state absorption (ESA) signal at 365 nm due to a red-shift of the reduced bpy^- cw-OA band with respect to the neutral one; iii) a very weak positive broadband signal at $\lambda > 500$ nm originating from transitions within higher excited MLCT states. Concerning the SVD result in panel B, as found in several metal-ligand complexes,[3] the first component (τ_1 ~110 fs) can be rationalized as the modulation of the charge density of the excited MLCT state due to solvation; the τ_3 component (τ_2 and τ_4 are kept only for consistency with the numbering from the analysis of the reference and of the dyad in the following panels but are not used) corresponds to spectral changes due to cooling, since ^{1}MLCT$\rightarrow$^{3}MLCT transition is excluded being pulse limited;[5] a very long-lived (τ_5) signal (infinity long-lived with respect to the time window spanned in this measurement) is assigned to the recovery of bpy^- GSB. No significant dynamics is observed in the region $\lambda > 550$ nm.

Moving to the reference system and the photoexcitation of Ru-to-phen MLCT states, we should observe first that the maximum of the absorption of neutral phen group is centred at 365 nm (see inverted OA bands in Figure S2C and compare with $[Ru(bpy)_3]^{2+}$ in Figure S2A).[6] Therefore, its

GSB, due to the photo-induced phen reduction, is expected in this region. Indeed, from comparing TA data of the reference with the $[Ru(bpy)_3]^{2+}$ ones (Figure S2 and Figure S4), we can identify in the earliest times a GSB signature at 350-390 nm that we can assign to the excitation of the Ru-to-phen MLCT state unit. This signal disappears in 2 ps and gives origin to a TA signal strongly resembling the one of the photo-excited $[Ru(bpy)_3]^{2+}$ (Figure S4). This is fully confirmed by the SVD-GF analysis (Figure S2B and D), where the only difference between the dynamical behaviour of the reference and of the $[Ru(bpy)_3]^{2+}$ dye is a biphasic decay with time constants of 140 fs and 2.85 ps of a negative signal at 365 nm and a positive contribution at 420-450 nm, as expected for a TA signal due to a red-shifted intra-ligand OA band of the reduced phen group.

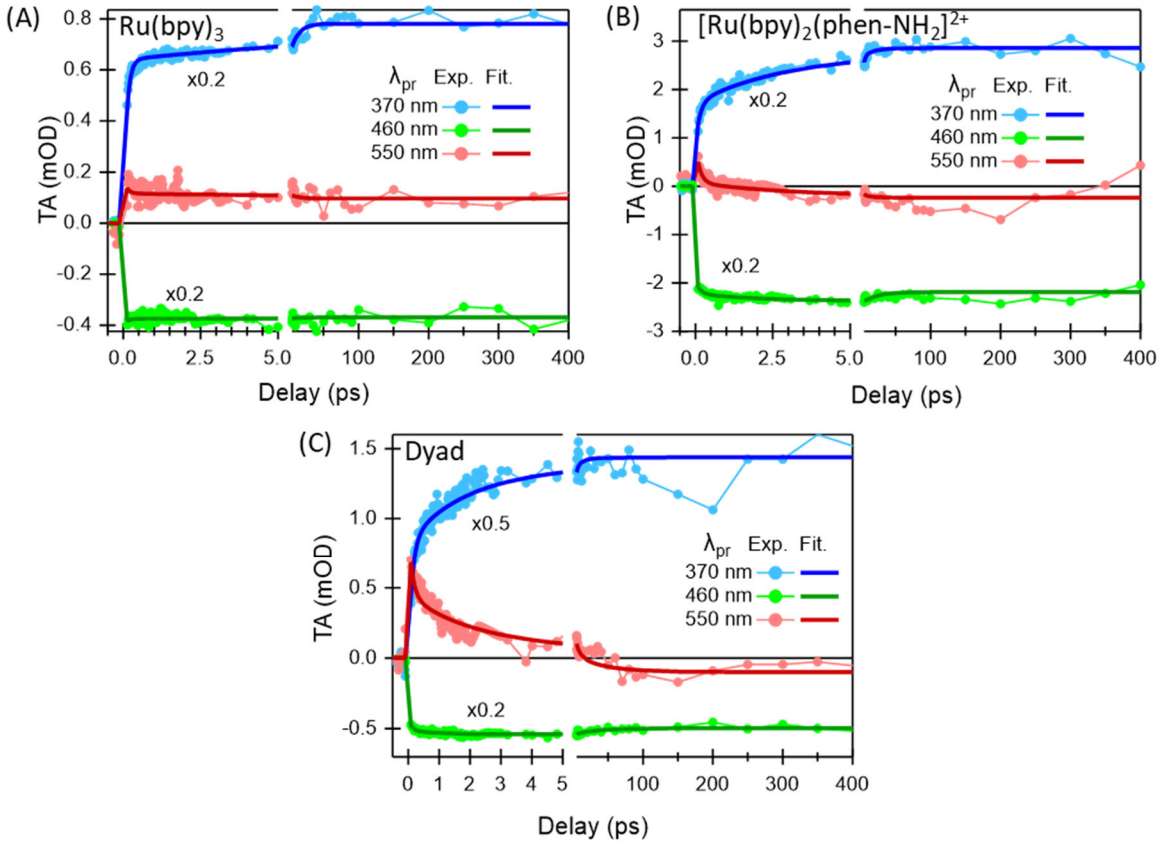

Figure S3: kinetics at relevant wavelengths (see Figure S2) upon excitation at 425 nm of $[Ru(bpy)_3]^{2+}$, $[Ru(bpy)_2(phen\text{-}NH_2)]^{2+}$ and the Ru(II)-Mo(VI) dyad (clockwise from top left panel, respectively). Kinetics at 370 nm and 460 nm report on the dynamics of the metal-to-ligand charge transfer states and of the the ground state bleach of the Ru moiety, respectively, whereas the one at and 550 nm shows the evolution of the oxidative process at the Mo unit. The kinetics reconstructed from the time-spectrum decomposition analysis (solid lines) are shown. It is worth noticing the quality of the fitting of the dyad at the wavelength representative of the oxidative process in panel C, is very good but not excellent. As commented in the main text this is a manifestation of the fact that the oxidation dynamics are multi-exponential and spanning from 2 to 60 ps.

These two components describe a spectral evolution which is consistent with a rise of the bpy^- ESA dynamics and decay of $phen^-$ GSB. The other components (τ_3 and τ_5) are the same as the respective ones for the $[Ru(bpy)_3]^{2+}$. These evidences clearly indicate that both Ru(III)-$phen^-$ and Ru(III)-bpy^- MLCT transitions can be excited at 425 nm and that the former is followed by a ligand-to-ligand charge transfer from the $phen^-$ to one of the neutral bpy on the ps timescale. A small red shift of the GSB at 450 nm in the reference with respect to the $[Ru(bpy)_3]^{2+}$ is measured consistently with the steady state measurements (compare the inverted OA bands in Figure S2 and TA spectra in Figure S4), while no stimulated emission is observed in agreement with its non-allowed character.[5] A similar behaviour is observed also in the dyad at $\lambda < 550$ nm (Figure S2E and F).

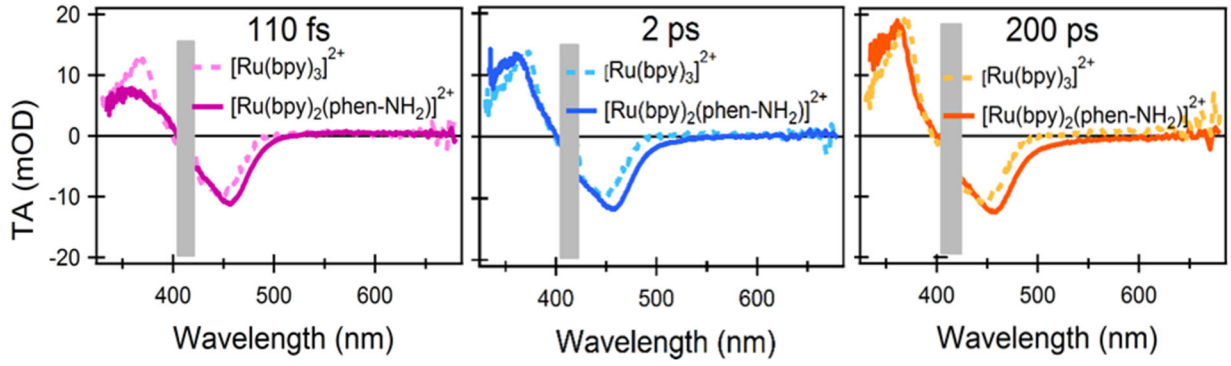

Figure S4: A comparison of $[Ru(bpy)_3]^{2+}$ and $[Ru(bpy)_2(phen\text{-}NH_2)]^{2+}$ spectra at different time delays. The spectral range contaminated by pump scattering is masked by a grey box.

The comparison of experimental data and of DASs from the dyad at different time delays with $[Ru(bpy)_2(phen\text{-}NH_2)]^{2+}$ (Figure S5) reveals also that the dyad signals at $\lambda > 500$ nm are dominated by transitions due to the Mo unit or the bridge. As discussed in the main text, these signals are due to ligand-centred transitions of the neutral Mo unit, which are red-shifted upon the strong electrostatic field generated by the photoinduced dipole on the Ru(III) unit. The origin of such a shift is ultimately a dynamical Stark effect[7] due to the appearing of a strong dipole (~ 10 D) on the close ruthenium unit. As shown by the comparison of the long-lived components from the reference and the dyad (Figure S5), the signal of neutral Mo(VI) unit disappears within the investigated time window (0-200 ps), in agreement with the formation of the charge separation state within this moiety and the bridge.

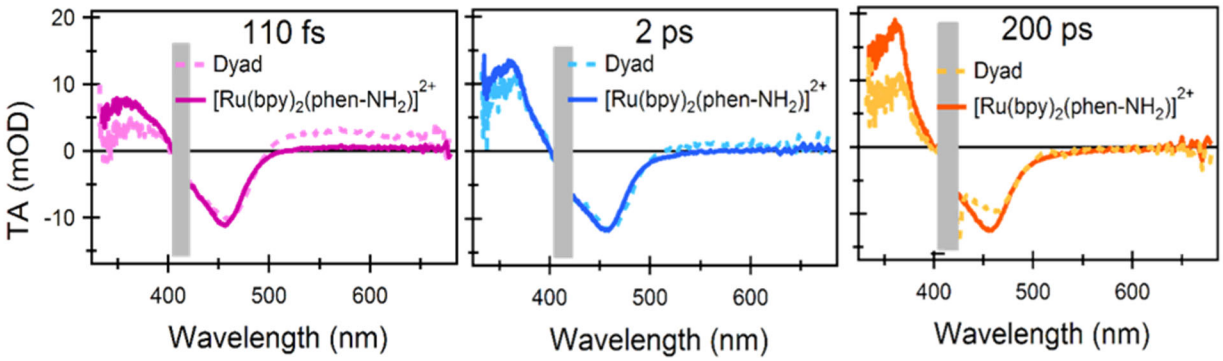

Figure S5: A comparison of dyad and $[Ru(bpy)_2(phen\text{-}NH_2)]^{2+}$ spectra at different time delays. The spectral range contaminated by pump scattering is masked by a grey box.

This comparison provides three key pieces of information: i) at the earliest time after excitation only the photoactive unit $[Ru(bpy)_2(phen\text{-}NH_2)]^{2+}$ is excited; ii) the signature of the ruthenium unit MLCT GSB is observed up to 200 ps which shows that the excited state of the photoactive unit is populated within the time window of measurements; iii) conversely, we observe the presence of two signals and dynamics at 380 nm and $\lambda > 500$ nm. As shown in the main text (see Figure 3 and relevant discussion) these differences are due to a charge redistribution from the Mo(VI) coordination ligand sphere towards acceptor orbitals on the non-innocent ligand close to the bridge or on the bridge itself.

3. Comparison of the Electrochemically-Oxidized Mo Moiety and Measurements of the Ru(II)-Mo(VI) Dyad upon Excitation at 450 nm

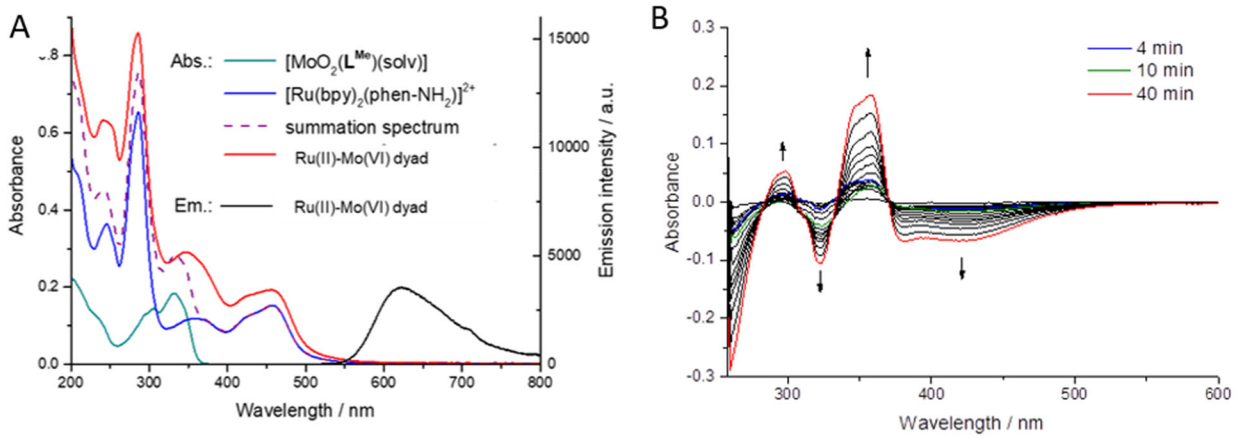

Figure S6: Comparison of the steady state absorption spectra of the Ru(II)-Mo(VI) dyad (red, solid line) with the ones of its isolated moieties (blue and cyan, solid lines) and of the their sum. For sake of completeness the phosphorescence of the dyad upon excitation at 450 nm is shown. b) Difference spectra obtained by electrochemical oxidation of [$MoO_2(L^{Me})$MeOH] (0.5 mM) recorded at E_{app}= 1.5 V after 1, 2, 3, 4, 6, 8, 10, 12, 15, 18, 21, 25, 30, 35, and 40 min (carbon veil electrode). Reproduced with permission from ref.[1].

In the main text we compared the electrochemical spectra (specifically the 4 min spectrum from (Figure S6B)) with TA results upon excitation at 425 nm. To provide further evidence that the spectral evolution at time longer than 2 ps is definitively due to the Mo unit, we performed the same measurements and analysis reported in the main text but upon excitation at 450 nm. At this wavelength we can indeed excite even more selectively the photoactive unit (Figure S6) and we have a clear detection range, not disturbed by the pump scattering, covering the maximum of the signal around 450 nm. The match of the spectro-electrochemical data[1] with the inverted sum -($DAS\tau_3$+$DAS\tau_4$) is excellent (Figure S7). All the main spectral features, including the sharp ones at 320 nm and the band at 350-370 nm, are perfectly reproduced. Remarkably the difference TA spectrum shows a negative structure absent both in the electrochemical spectra and in the sum –($DAS\tau_3$+$DAS\tau_4$). The comparison with the sum –($DAS\tau_2$ +$DAS\tau_3$+$DAS\tau_4$) reveals that this contribution is due to the GSB dynamics of the ruthenium unit related to the $phen^-$ to bpy^- charge transfer process, described indeed by the second DAS in Figure S2D.

Therefore, we can state that the results discussed in the main text are confirmed regardless of the excitation wavelength, at least within the MLCT band of the ruthenium unit.

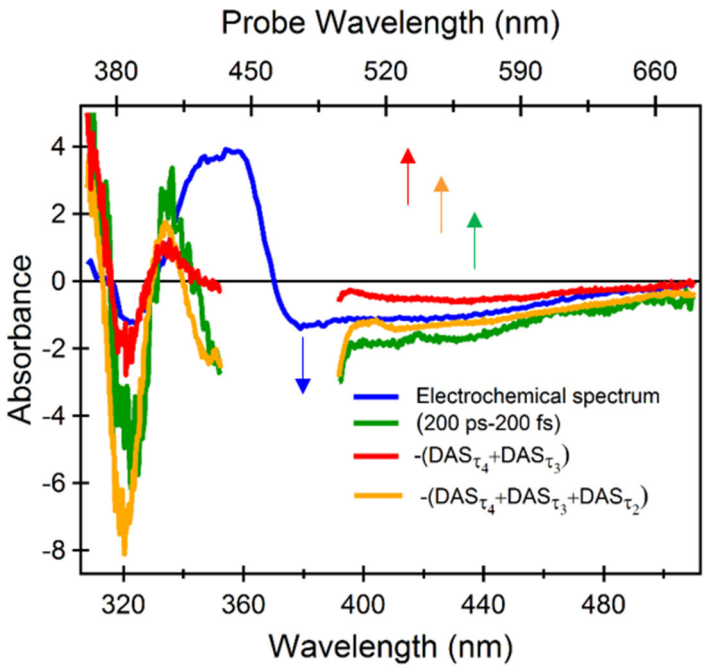

Figure S7: Comparison of the signal of the oxidized Mo unit obtained by spectro-electrochemical oxidation of $[MoO_2(L^{Me})MeOH]^1$ (blue) with the time-resolved signals recorded upon excitation of the Ru(II)-Mo(VI) dyad at 450 nm (green) and with the related SVD-GA spectral components (see also Figure S1B and Figure 3B)); the difference TA spectrum at 200 ps with respect to 200 fs, the inverted sum $-(DAS\tau_3+DAS\tau_4)$ (red) and, for sake of completeness, also the inverted sum $-(DAS\tau_2+DAS\tau_3+DAS\tau_4)$ (yellow). As in Figure 3B, to compare the two set of spectra a relative shift of 0.65 eV was applied in energy domain.

4. Possible implications for the Photo-Induced Oxidation-Enhancing Effect on Longer Timescales (>ns)

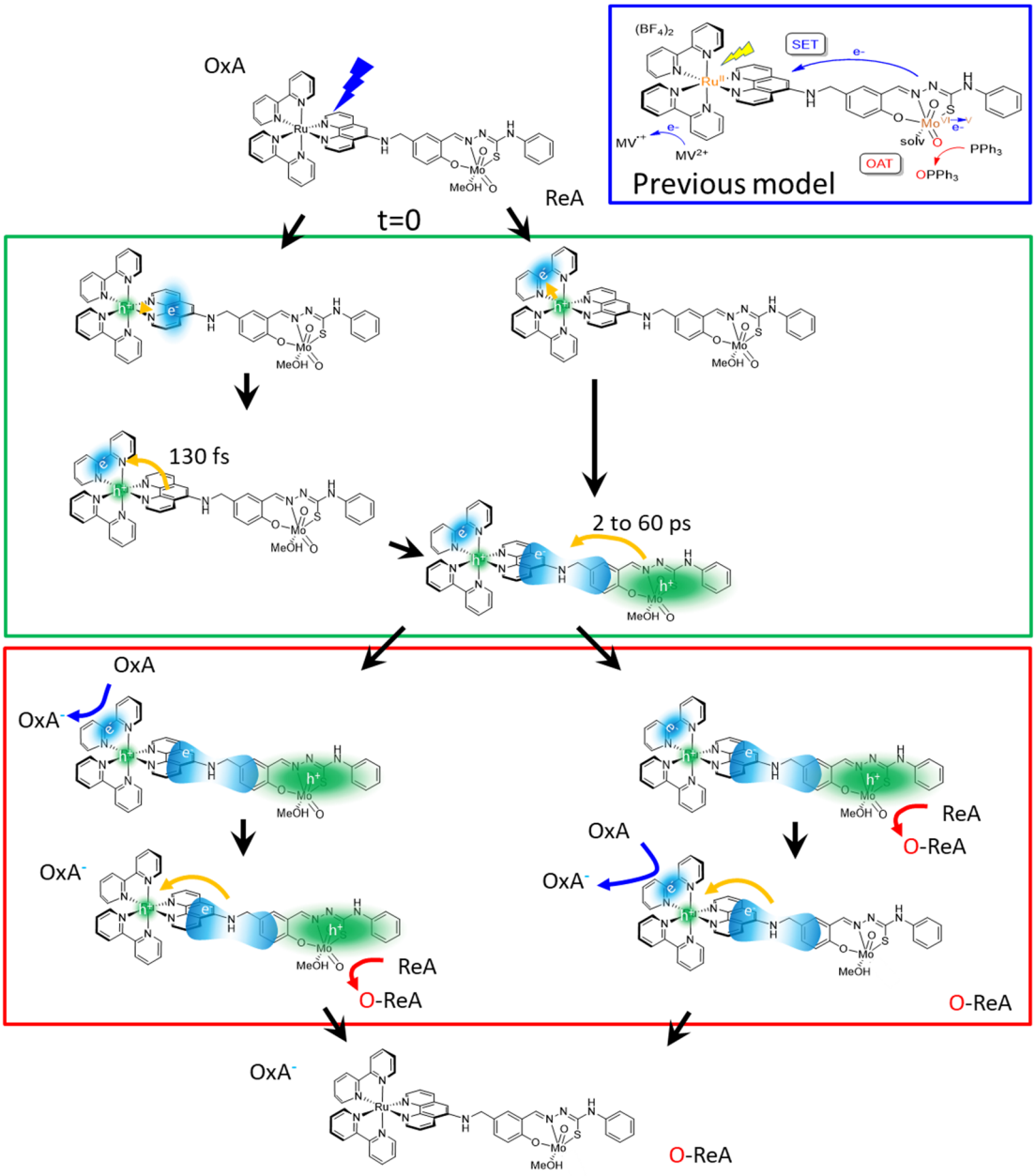

Figure S8: The previous and the new model for the photo-induced oxidation-enhancing (PIOE) effect are both shown (blue and green boxes, respectively). A potential reaction model for longer timescales is also proposed (red box). Figure only shows the oxidative path of the catalytic cycle (the reaction with the oxygen atom acceptor PPh_3), which is shown for sake of completeness in Figure S9.

According to the new model for the photo-induced oxidation-enhancing (PIOE) effect derived in the main article (green box in Figure S8), the initial step of the PIOE process is not diffusion-limited, but it is due to an intramolecular electron redistribution, from the Mo unit towards the bridging groups immediately after photo-oxidation of Ru(II) to Ru(III). Therefore, the Ru(II)-Mo(VI) dyad is photoexcited in a state where both functional components are potentially activated (the bpy is reduced and the total charge of the Mo coordination ligand sphere is decreased) and coexist in the same system, whereas the electron from the Mo unit is not yet localized on the ruthenium unit (or at least its localization does not cause any detectable distortion). This unique excited state of the supramolecular system is depicted by the bottom scheme inside the green box of Figure S8. We have not carried out any further experimental or theoretical investigation to track down the subsequent reactions, but a plausible scenario is depicted inside the red box; since the two reaction centres are simultaneously active, both the neutralization of charge on the bpy by the oxidizing agent and the reduction of Mo by the reducing agent can happen in parallel. The presence of the oxidizing agent is not necessary for the initial activation of the Mo unit (see the old model framed in the blue box of Figure S8) but to regenerate it via two parallel paths; either oxidation of bpy^- and then reduction of Mo or vice versa. Which of the two routes will be the dominant one depends on the ratio between the oxidizing and reducing reaction rates. The case discussed in the article,[1] where the OAT process is several orders of magnitude slower than the oxidation of the bpy^- ligand would correspond to the left branch.

For sake of completeness, the full catalytic cycle is sketched in Figure S9.

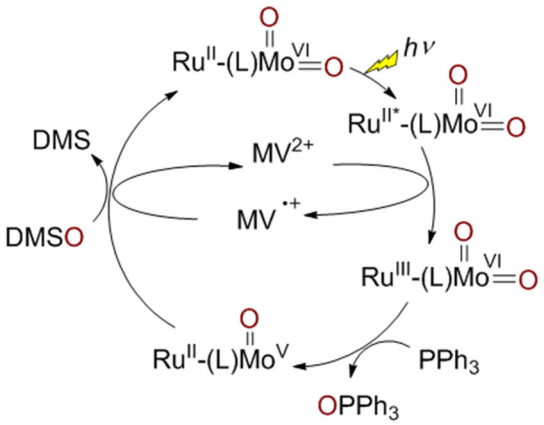

Figure S9: The proposed full catalytic cycle of the Ru-Mo dyad: the dyad is regenerated by oxygen atom donation from DMSO, the oxo-donor closing the catalytic process. Figure S8 only shows the oxidative half of the catalytic cycle (the reaction with the oxygen atom acceptor PPh_3). Methyl viologen (MV^{2+}) is only a mediator, it is regenerated in the process. The cycle should be as the one in the Figure, except that real

oxidation states of the intermediate species are not known yet. Reproduced with permission from ref.[1].

References:

1 A. B. Ducrot, B. A. Coulson, R. N. Perutz and A.-K. Duhme-Klair, *Inorg. Chem.*, 2016, **55**, 12583–12594.

2 M. Nazari, C. D. Bösch, A. Rondi, A. Francés-Monerris, M. Marazzi, E. Lognon, M. Gazzetto, S. M. Langenegger, R. Häner, T. Feurer, A. Monari and A. Cannizzo, *Phys. Chem. Chem. Phys.*, 2019, **21**, 16981–16988.

3 A. Cannizzo, A. M. Blanco-rodríguez, A. El Nahhas, J. Šebera, S. Záliš, A. Vlček Jr. and M. Chergui, *J. Am. Chem. Soc.*, 2008, **130**, 8967–8974.

4 A. N. Tarnovsky, W. Gawelda, M. Johnson, C. Bressler and M. Chergui, *J. Phys. Chem. B*, 2006, **110**, 26497–26505.

5 A. Cannizzo, F. van Mourik, W. Gawelda, G. Zgrablic, C. Bressler and M. Chergui, *Angew. Chem. Int. Ed.*, 2006, **45**, 3174–3176.

6 S. Záliš, C. Consani, A. El Nahhas, A. Cannizzo, M. Chergui, F. Hartl and A. Vlcek Jr., *Inorganica Chim. Acta*, 2011, **374**, 578–585.

7 M. Meister, B. Baumeier, N. Pschirer, R. Sens, I. Bruder, F. Laquai, D. Andrienko and I. A. Howard, *J. Phys. Chem. C*, 2013, **117**, 9171–9177.